Electric Power Systems Research 230 (2024) 110262

Contents lists available at ScienceDirect

Electric Power Systems Research

journal homepage: www.elsevier.com/locate/epsr

Thermal model of DC conductors for railway traction networks: A hosting capacity assessment

Mohammed G. Mahairi [a], Bassam Mohamed [a,1], Pablo Arboleya [b,*,2]

[a] R&D Department at Plexigrid, Spain
[b] Department of Electrical Engineering, University of Oviedo, Spain

ARTICLE INFO

Keywords:
DC railway traction
Cable thermal rating
Bare conductors thermal rating
Hosting capacity

ABSTRACT

In this paper, the authors have adapted existing thermal models for the calculation of conductor temperature for use in electrical distribution systems for railway applications in multi-train environments. For this purpose, the authors have used existing standards such as IEEE 738 for overhead lines and have proposed a resolution methodology based on the difference equation model for cables. The authors have opted for a simplified method since the priority in this case is the resolution in systems with multiple stations, lines, and trains. For this same reason, they have chosen to decouple the electrical and thermal calculations so that the electrical variables calculated through load flows constitute the input to the thermal calculation problem. The paper reviews the existing formulation and proposes models for specific use in railway applications in a multi-train environment. A detailed analysis of the results obtained in a real case study is presented as a validation element.

1. Introduction

The current increase in the world population introduces new challenges to various sectors, including railway systems. There is a need to create a transportation system capable of carrying enormous quantities of passengers and commodities while decreasing environmental effects. Railway transportation emits 3–10 times less CO_2 than road or air travel, and rail uses roughly 3.5 times less land per passenger-kilometer than vehicles [1]. As a result, railways are considered more sustainable than other modes of transport. According to [1], in 2030, the length of high-speed railway networks is expected to triple what it was in 2015, covering the majority of passengers in the intermediate distance. In 2050, more than half of all products transported by road will be transported by rail or ship over ranges of more than 300 kilometers [1]. In anticipation of this encouraging scenario, it is essential to design and study new networks, as well as to expand existing ones. The thermal behavior of power cables determines the limitation of power flow through them, which in turn limits the number of trains in a network. Static thermal analysis produces very reliable results, but underestimates the true potential of a network. To increase efficiency and unlock the full potential of exciting networks, dynamic thermal analysis is necessary. This takes into account many aspects, such as weather conditions. Accurate identification of conductor thermal profiles will provide critical information for network control strategies, including operating condition monitoring, lifetime estimation, ampacity assessment, and load forecasting and management. To investigate thermal analysis in rail traction networks, the thermal behavior of bare overhead lines and cables is further examined. Numerous studies have investigated how to calculate the transient temperature of a bare overhead conductors taking into account various materials and structural features that impact heat transfer. For instance, researchers in [2–4] used a thermal circuit model to develop a temperature calculation model based on the theory of thermal-electrical analogies. This model incorporates heat transfer analysis into an electrical circuit solution, enabling a simple and effective understanding of how an overhead transmission line works while considering the heat transfer properties of different materials. However, this model does not account for temperature-dependent features of various conductor properties during dynamic thermal processes. Other studies, such as [5–7], developed radial or axial temperature calculation models based on the concept of thermal equilibrium and constant ambient temperature and humidity. These models accurately calculate the radial and axial temperature distributions of a conductor under ideal natural convective heat transfer conditions. However, transmission lines typically operate in a more complex environment with forced convective heat transfer scenarios affected by various factors like wind and solar radiation. Therefore, the calculation technique based on ideal natural convection circumstances

* Corresponding author.
E-mail addresses: mohammed.mahairi@plexigrid.com (M.G. Mahairi), bassam@plexigrid.com (B. Mohamed), arboleyapablo@uniovi.es (P. Arboleya).
[1] Member, IEEE.
[2] Senior Member, IEEE.

https://doi.org/10.1016/j.epsr.2024.110262
Received 16 November 2023; Received in revised form 15 February 2024; Accepted 20 February 2024
Available online 23 February 2024

cannot fully capture the impact of the ambient environment on the conductor's temperature. Some studies have used a finite element model to solve the transient temperature field of conductors [8]. Nevertheless, the accuracy of this model depends on the grid size and structural division, and it requires significant computation time, making it unsuitable for meeting the timing constraints of power system protection. When studying the thermal properties of power cables and overhead lines, analytical and numerical methods are commonly used [9]. Analytical methods are limited in their ability to account for material homogeneity and cable architecture [10]. Numerical approaches, such as the Finite Difference Method (FDM) [11,12], Finite Element Method (FEM) [13–15], and Thermal-Electrical Equivalent (TEE) [16], are preferred for calculating temperature distribution within the cable and its external environment. Both FDM and FEM methods increase solution speed as the number of points studied decreases, but this comes at the cost of solution accuracy [11]. In-homogeneous materials can be considered in both methods, but only FEM allows the modeling of complex scenarios. Moreover, other numerical approaches are available for more complex scenarios such as the Volume Element Method, which is used mainly for charge transport in a cables [17], High-Temperature Superconducting (HTS) cables [18–22], and Gas-Insulated Lines (GIL) [23]. TEE, as a technique, shares many similarities with FDM [24,25]. It utilizes the analogies between heat transfer and electrical equations to model the system. To simulate cables and the surrounding environment, capacitors, resistors, and generators are used. Thermal resistance is the ratio of the temperature difference across a material to the rate of heat transfer per unit area, while thermal capacitance measures a material's capacity to store heat. This paper addresses the dynamic thermal analysis of DC railway traction networks. This analysis will be applied to all current-carrying conductors, including catenary lines, feeders, power injection wires, and cross-coupling between catenary lines. Those conductors could be bare or insulated (cables) whether underground or in the air. The method used in this paper aims to accurately get the transient thermal behavior in a faster and simpler way to be used by railway applications. The purpose of this application is to utilize the full potential of current railway networks, and help in the planning process maximizing the hosting capacity. The proposed model is ready to be used in complex multi-train simulation tools like the ones proposed by the authors in their previous works [26,27] and thus, accurately estimate the hosting capacity of the grid considering the real temperature of all sections and not only steady-state estimations. In order to finalize this introductory part, the authors would like to emphasize that the contribution of the paper has to do precisely with the application of the existing thermal models for the specific application of the calculation of railway distribution systems, and the proposal of a solving procedure by applying the differential equation model adapted to a multi-train environment, which has not been done before. This allows the authors to continue advancing in the line of research related to the mechanical-electrical decoupled modeling of railway distribution systems adding the thermal modeling layer.

2. Thermal model of bare overhead conductors

The mathematical model used to analyze bare overhead conductors is based on the IEEE 738-2023 standard [28]. This standard uses the modified House and Tuttle method [29] to calculate the current-temperature relationship of bare overhead conductors. The numerical thermal model provided in this standard is comprehensive and can be used for both steady-state and dynamic calculations. All the critical factors are taken into account in this method without any simplifications. It is important to state that the mathematical model presented by this standard is used directly in the developed thermal calculation methodology without modification. In this section, the authors provide a brief explanation of the IEEE 738 standard's model. The temperature of the conductor is dependent on various factors, including the electrical resistivity and heat capacity of the conductor, the diameter of the conductor, the emissivity and absorptivity of the conductor surface, the weather conditions (such as air temperature, solar heating, wind speed, and wind direction), and the current flowing through the conductor. In order to get the change in temperature at each time instant, the heat balance (1) for the conductor must be solved.

$$\begin{aligned} &q_c + q_r + m \cdot C_p \cdot \frac{dT_c}{dt} = q_s + I^2 \cdot R(T_c) \\ &\frac{dT_c}{dt} = \frac{1}{m \cdot C_p} \cdot [I^2 \cdot R(T_c) + q_s - q_c - q_r] \end{aligned} \tag{1}$$

Where T_c is the conductor temperature, $\frac{dT_c}{dt}$ is the change of conductor temperature with time. The convective heat loss rate is represented by q_c, the radiated heat loss rate is represented by q_r, and the solar heat gain rate is represented by q_s. The thermal heat capacity of the conductor is represented by $m \cdot C_p$, where m is the mass of the conductor and C_p is the specific heat capacity of the conductor. The current passing through the conductor is represented by I, and the temperature-dependent resistance of the conductor is represented by $R(T_c)$. The methods of calculating each variable in the heat balance equation presented above and the required inputs will be discussed briefly in the next paragraphs. More details on the implementation are found in [28].

2.1. Convective heat loss rate (q_c)

Heat loss through convection can be classified as either natural convection or forced convection. The magnitude of convective heat loss is determined by a dimensionless parameter known as the Reynolds number, which is given in (2):

$$N_{Re} = \frac{D_0 \cdot \rho_f \cdot V_w}{\mu_f} \tag{2}$$

Reynolds number is a function of air density ρ_f, the dynamic viscosity of air μ_f, conductor diameter D_0, and wind velocity V_w. The method of calculating each of the aforementioned quantities is explained extensively in [28]. It is recommended for calculating the convection heat loss to calculate both the natural and forced convection heat loss. The natural convection q_c can be calculated using (3).

$$q_{cn} = 3.645 \cdot (\rho_f)^{0.5} \cdot (D_0)^{0.75} \cdot (T_c - T_a)^{1.25} \tag{3}$$

There are two equations to calculate the forced convection heat loss as can be seen in (4) and (5). (4) is accurate at low wind speeds, but it loses this accuracy at high wind speeds. Oppositely, (5) is accurate at high wind speeds and not accurate at low wind speeds.

$$q_{c1} = K_{angle} \cdot \left[1.01 + 1.35 \cdot (N_{Re})^{0.52}\right] \cdot k_f \cdot (T_c - T_a) \tag{4}$$

$$q_{c2} = K_{angle} \cdot 0.754 \cdot (N_{Re})^{0.6} \cdot k_f \cdot (T_c - T_a) \tag{5}$$

K_{angle} is the wind direction factor, and T_a is the ambient temperature. (6) shows the method of calculating K_{angle}. where ϕ is the angle between the conductor axis and the wind direction. Its value ranges between 0° (parallel) and 90° (perpendicular).

$$K_{angle} = 1.194 - \cos(\phi) + 0.194 \cdot \cos(2\phi) + 0.368 \cdot \sin(2\phi) \tag{6}$$

IEEE 738 standard recommends calculating the rate of heat loss due to forced convection using both equations and selecting the higher value. Then, the convective heat loss rate q_c will be the highest between nature and forced convection. In a nutshell, $q_c = MAX(q_{cn}, q_{c1}, q_{c2})$.

2.2. Radiated heat loss rate (q_r)

The radiated heat loss rate is calculated by using (7).

$$q_r = 17.8 \cdot D_0 \cdot \epsilon \cdot \left[(\frac{T_c + 273}{100})^4 - (\frac{T_a + 273}{100})^4 \right] \tag{7}$$

Where ϵ is the emissivity of the conductor. It ranges between (0.23 to 0.91) and it changes with time. The constant value (17.8) contains Stefan–Boltzmann constant [30] and a conversion factor to get the result in (W/m).

Table 1
Electro-thermal analogy [32].

Electrical	Symbol	Thermal	Symbol
Resistance	R[Ω]	Resistance	T[m K/W]
Current	I[A]	Heat flow	W_{loss}[W/m]
Capacitance	C_e[F]	Capacity	C[J/(m K)]
voltage	U[V]	Temperature	θ[K]

2.3. Rate of solar heat gain (q_s)

The rate of solar heat gain can be calculated using (8).

$$q_s = \alpha \cdot Q_{se} \cdot \sin(\theta) \cdot A' \tag{8}$$

Where α is the absorptivity of the conductor's surface, which ranges between (0.23 to 0.91), Q_{se} is total heat flux density, A' is the projected area, and θ is the effective angle of incidence of the sun's rays. The method of calculating each of the aforementioned quantities is explained extensively in [28]. It is worth mentioning that Q_{se} counts for both, the elevation of the conductor from sea level and the amount of atmospheric attenuation (pollution, cloud cover, and moisture). It is the result of the multiplication of solar heat intensity Q_s and solar flux elevation correction K_{solar} as follows:

$$Q_{se} = Q_s \cdot K_{solar} \tag{9}$$

2.4. Conductor electrical resistance ($R(T_c)$)

Conductor electrical resistance is found by linear interpolation according to (10). Where $R(T_{high})$ and $R(T_{low})$ represent the higher and lower resistance values of the conductor.

$$R(T_c) = \frac{R(T_{high}) - R(T_{low})}{T_{high} - T_{low}} \cdot [T_c - T_{low}] + R(T_{low}) \tag{10}$$

2.5. Conductor heat capacity ($m \cdot C_p$)

This quantity is important in the thermal modeling of power cables and overhead lines since it determines the amount of heat required to increase the temperature of the conductor by a certain amount. The heat capacity per unit length is calculated by multiplying the specific heat of the conductor material by the mass per unit length. If the conductor is made up of multiple materials, the heat capacity is the sum of the heat capacities of all the individual materials as in (11). This value is crucial in accurately predicting the temperature response of a cable or overhead line to changing environmental and operational conditions.

$$m \cdot C_p = \sum m_i \cdot C_{pi} \tag{11}$$

3. Thermal model of insulated wires (Cables)

The Thermal-Electrical Equivalent (TEE) method is a popular choice for analyzing cable systems due to its ability to handle complex cable designs in a convenient manner [31]. This approach, uses an electrical circuit as an analogy to represent the thermal circuit, where heat flow is analogous to electrical current and temperature is analogous to voltage. If the thermal parameters are independent of temperature, the electrical circuit is linear. The superposition principle is used to address heat transfer problems using this method [31]. The standard thermal models of cables are developed using the thermal-electrical analogy presented in Table 1.

The temperature of the system is represented by the electric potential at different nodes, and the heat flows are calculated using an RC circuit. Typically, the length of the cable is considered to be substantially longer than its diameter [16]. Moreover, there are no axial fluctuations, and the heat flux is distributed exclusively in the radial direction [16]. Furthermore, when the heat source is placed on the conductor's outer portion, the thermal resistance of the conductor is ignored.

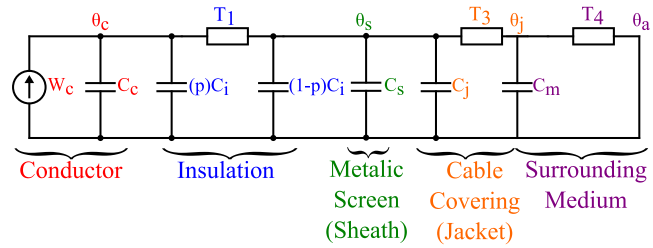

Fig. 1. Thermo-electric equivalent (TEE) of a DC cable.

The TEE model that will be used in this paper is adapted from [31] and used by [24,25,33–37]. These authors have used a model considering AC cables with insulation and sheath losses. Other publications have studied the effects of DC cables as in [38,39] or combined AC and DC cables such as the authors of [40]. In contrast to AC cables, DC cables do not experience dielectric or screen loss, because there is no current circulation in the insulating dielectric and metallic screen while transmitting direct current [34]. Therefore, a simplified unarmored DC cable model is shown in Fig. 1.

The figure includes various parameters that denote different aspects of the thermal behavior of the cable. C_c represents the thermal capacitance of the conductor, C_i represents that of the insulation, C_s represents that of the screen, C_j represents that of the jacket, and C_m represents that of the medium surrounding the cable. The Joule's loss in the conductor is represented by W_c. T_1 represents the thermal resistance per unit length between the conductor and the sheath, T_3 represents the thermal resistance per unit length of the external serving or jacket, and T_4 represents the thermal resistance per unit length between the cable surface and the surrounding medium. The Van Wormer coefficient is represented by p, and its significance is explained in later sections. The temperature of the conductor, screen, jacket, and ambient are represented by θ_c, θ_s, θ_j, and θ_a, respectively. The equation provides a comprehensive representation of the thermal behavior of cables and their surroundings. The voltage at any point of an electric circuit is measured or calculated as a difference from a known reference point (usually the ground is considered the reference). Thus, the temperature at any point should be calculated in regard to a reference temperature, which will be the ambient temperature θ_a in this model. The lumped parameter network model of the cable system is used to develop both steady-state and transient rating equations. However, there are significant differences between these two equations [31].

3.1. Internal thermal resistances

The internal thermal resistances and capacitances of a cable are properties that depend on the construction of that cable. It can be assumed, that these quantities are constant and independent of the component temperature according to [31] without loss of accuracy. The calculation method of thermal resistances is taken from the second part of IEC 60287 standard [41]. According to this standard, and to be consistent with TEE of Fig. 1, metallic tapes are treated as a part of the conductor or sheath in thermal calculations when screening layers are present. Oppositely, semi-conducting layers (including metalized carbon paper tapes) are treated as a part of the insulation. The relevant component dimensions must be updated as a result.

The scope of this model considers only single-core cables that are directly buried in soil, exposed to air, or inside a duct. Thus, the discussion of thermal resistances will be limited to those scenarios. [41] provides the calculation methods of various cable constructions and installations.

3.1.1. Thermal resistance between conductor and sheath T_1

The thermal resistance of the insulation dielectric between the conductor and sheath can be calculated using the following formula:

$$T_1 = \frac{\rho_i}{2\pi} \ln\left(\frac{d_i}{d_c}\right) \tag{12}$$

d_c and d_i are the outer and inner diameters of the insulation layer, respectively. ρ_i is the thermal resistivity of insulation.

3.1.2. Thermal resistance of outer covering (Jacket) T_3

The thermal resistance of the jacket is calculated from:

$$T_3 = \frac{\rho_j}{2\pi} \ln\left(\frac{D_e}{d_s}\right) \tag{13}$$

Where ρ_j is the thermal resistivity of the jacket, and d_s is the outer diameter of the sheath.

3.2. External thermal resistance

The thermal resistance of the material surrounding the cable, denoted as T_4, plays a crucial role in determining the current-carrying capacity of cables. When cables are buried underground, T_4 contributes to more than 70% of the temperature rise in the conductor. The external thermal resistance in underground installations is influenced by several factors, including the cable diameter, depth of laying, method of installation, heat produced by adjacent cables, and thermal properties of the soil. In aerial cables, the impact of external thermal resistance on cable rating is lower than that of underground cables. The installation conditions (such as indoor or outdoor placement, and proximity to walls or other cables) significantly affect the calculation of external thermal resistance for aerial cables. These observations were made by Anders in [31].

3.2.1. Cables in air protected from direct solar radiation

The external thermal resistance (T_4) of a cable in the air not exposed to sunlight is given by:

$$T_4 = \frac{1}{\pi \cdot D_e \cdot h \cdot (\Delta\theta_z)^{1/4}} \tag{14}$$

Where h is the heat dissipation coefficient, that is obtained for single core cable from:

$$h = \frac{0.21}{(D_e)^{0.6}} + 3.94 \tag{15}$$

$\Delta\theta_z$ is the excess of cable surface temperature above θ_a. It can be calculated using the iterative technique of (16), where the initial value is $(\Delta\theta_z)^{1/4} = 2$ and iteration process continues until $(\Delta\theta_z)^{1/4}_{n+1} - (\Delta\theta_z)^{1/4}_n \leq 0.001$.

$$(\Delta\theta_z)^{1/4}_{n+1} = \left(\frac{\Delta\theta_c}{1 + K_a \cdot (\Delta\theta_z)^{1/4}_n}\right)^{0.25} \tag{16}$$

Where:

$$K_a = \pi \cdot D_e \cdot h \cdot \left(\frac{T_1}{n} + T_2 + T_3\right) \tag{17}$$

3.2.2. Cables in air directly exposed to solar radiation

The external thermal resistance T_4^* of a cable directly exposed to solar radiation is computed from (14). The only difference is in the calculation method of $(\Delta\theta_z)^{1/4}$ as shown:

$$(\Delta\theta_z)^{1/4}_{n+1} = \left(\frac{\Delta\theta_c + \Delta\theta_{solar}}{1 + K_a \cdot (\Delta\theta_z)^{1/4}_n}\right)^{0.25} \tag{18}$$

Where:

$$\Delta\theta_{solar} = \sigma \cdot D_e \cdot H_{solar} \cdot \left(\frac{T_1}{n} + T_2 + T_3\right) \tag{19}$$

3.2.3. Single isolated buried cable

The external thermal resistances of cables directly buried in the soil is obtained from:

$$T_4 = \frac{\rho_{soil}}{2\pi} \ln\left(u + \sqrt{u^2 - 1}\right) \tag{20}$$

$$u = \frac{2 \cdot L}{D_e} \tag{21}$$

The distance between the cable surface and the surrounding medium is represented by L. The thermal resistivity of the soil is denoted by ρ_{soil}. When the value of the dimensionless parameter u exceeds 10, the following equation provides a reasonable estimate for T_4:

$$T_4 = \frac{\rho_{soil}}{2\pi} \ln\left(2 \cdot u\right) \tag{22}$$

3.2.4. Cables in ducts or pipes

The thermal resistance outside a cable installed in a duct is categorized into three components. The initial component is the thermal resistance due to the air gap between the cable's surface and the interior surface of the duct or pipe (T_4'). This component can be computed using the following formula:

$$T_4' = \frac{U}{1 + 0.1 \cdot (V + Y \cdot \theta_m) \cdot D_e} \tag{23}$$

U, V, and Y are coefficients that are determined by the installation method, and their values can be found in [41]. To compute the thermal resistance between the cable and the duct, an initial value for the average temperature of the medium θ_m must be assumed, and the calculation may need to be iterated with a revised value if necessary.

The second component of the external thermal resistance of a cable is the thermal resistance of the duct or pipe. It is calculated in the same way as the insulation and jacket, as shown below, according to [41]:

$$T_4'' = \frac{\rho_{duct}}{2\pi} \ln\left(\frac{d_{de}}{d_{di}}\right) \tag{24}$$

Where ρ_{duct} is the thermal resistivity of duct material, d_{de} is the duct external diameter, and d_{di} is the duct internal diameter. For metal ducts or pipes, ρ_{duct} can be considered as zero and the thermal resistance of the duct itself (T_4'') is negligible [41].

The last part is the external thermal resistance of the duct or pipe (T_4'''). It is calculated depending on duct (or pipe) installation whether above ground or underground. Eqs. (14) and (20) are used, but with replacing the external diameter of a cable D_e with the external diameter of the duct or pipe d_{de}. Finally, The external thermal resistance of a cable in a duct or pipe is:

$$T_4 = T_4' + T_4'' + T_4''' \tag{25}$$

3.3. Mathematical modeling

A mathematical model is needed to solve the differential equations of the TEE circuit in all cases. The "Difference Equation" methodology is utilized by this paper. A description of the methodology that starts from the thermal circuit to the difference equation is explained in this section.

3.3.1. State-space representation

A system that changes in time following a fixed rule is called a dynamic system. Many systems, including the system proposed, are governed by a set of first-order differential equations in the form of (26) [42].

$$\dot{x} = \frac{dx}{dt} = f\,(x(t), u(t)) \tag{26}$$

In a control system, the state vector $x(t)$ is a set of variables that describes the system's state or configuration at a given time t. The vector $u(t)$ represents the external inputs to the system at that time, and the function f calculates the time derivative of the state vector at a specific time.

By integrating (26), according to [42], knowing the starting state $x(t_0)$ and the inputs' time history $(u(t))$ between t_0 and t_1 allows us to accurately calculate the state vector at any given moment $(x(t_1))$. To capture the behavior of a given system (solve the state equations), a minimum number of state variables (n) is necessary. The dimensionality of the state space is determined by n, which is referred to as the system order. In the proposed model, the system order corresponds to the number of non-parallel capacitors, for example, in Fig. 1 the system order is $n = 4$. For continuous linear time-invariant (LTI) systems with [system order $= n$, number of inputs $= p$, number of outputs $= q$], the standard state-space representation is given by [42]:

$$\dot{\mathbf{x}} = A\mathbf{x} + B\mathbf{u} \tag{27}$$

$$\mathbf{y} = C\mathbf{x} + D\mathbf{u} \tag{28}$$

In the given equation, $\mathbf{x}$ denotes a vector comprising n state variables with dimensions of $n \times 1$. The time derivative of the state vector is represented by $\dot{\mathbf{x}}$, which is also an $n \times 1$ vector. $\mathbf{u}$ is a vector with dimensions of $p \times 1$, representing external input to the system. $\mathbf{y}$ is a vector of output with dimensions of $q \times 1$. The system matrix is represented by A, which is an $n \times n$ matrix. B is the input matrix with dimensions of $n \times p$. C is the output matrix with dimensions of $q \times n$, and D is the feed-forward matrix with dimensions of $q \times p$. C is used to choose which state variables are required as an output, which in our case is only the conductor temperature. D is non-zero if outputs are related directly to inputs, which is not our case, where outputs are related to inputs through state variables not directly.

3.3.2. Transfer function representation

According to [42], it is possible to use the Laplace transform to transform the time-domain description of a system into a frequency-domain representation of input/output, called the transfer function. It also simplifies the analysis and evaluation of the governing differential equation by converting it to an algebraic equation. A general form of a transfer function is shown below:

$$G(s) = \frac{Y(s)}{U(s)} = \frac{b_m s^m + b_{m-1} s^{m-1} + \cdots + b_1 s + b_0}{a_k s^k + a_{k-1} s^{k-1} + \cdots + a_1 s + a_0} \tag{29}$$

The coefficients of the numerator and denominator polynomials of the transfer function, denoted as $b_0, b_1, \dots, b_m$ and $a_0, a_1, \dots, a_k$ respectively, can be used to compute the Laplace transform of the input $u(t)$ to the output $y(t)$ using the Laplace transforms $U(s)$ and $Y(s)$. The transfer function can also be obtained from the state-space representation using the given equation:

$$G(s) = \frac{Y(s)}{U(s)} = C(s\mathbf{I} - A)^{-1} B + D \tag{30}$$

The transfer function using the Laplace transform can be transformed to a discrete form in z-transform by replacing the Laplace operator with $[s \longrightarrow (z-1)/(z+1)]$. A general form of a transfer function using z-transform for the case of the thermal circuit with [system order $= n$] is shown below:

$$\begin{aligned} H(z) = \frac{Y(z)}{U(z)} &= \frac{b_n z^n + b_{n-1} z^{n-1} + \cdots + b_0}{a_n z^n + a_{n-1} z^{n-1} + \cdots + a_0} \\ &= \frac{b_n + b_{n-1} z^{-1} + \cdots + b_0 z^{-n}}{a_n + a_{n-1} z^{-1} + \cdots + a_0 z^{-n}} \end{aligned} \tag{31}$$

3.3.3. Difference equation representation

The difference equation describes the relationship between an input signal $u[k]$ and an output signal $y[k]$ over discrete time periods, where k is the sample index [42]. $y[k]$ reflects the value of the output at time kt_s, where t_s is a constant sample time (in this model $t_s = 1$ s). Using the difference equation, the output signal $y[k]$ is calculated using the present and past values of the input ($u[0]$ to $u[k]$), and past values of the output ($y[0]$ to $y[k-1]$) [42]. The difference equation is obtained from the discrete transfer function after transforming it back to the time domain. In time-domain, z^{-m} means the value before m sample times (mt_s). For example, $Y(z) \cdot z^{-1} \rightarrow y[k-1]$, $Y(z) \cdot z^{-n} \rightarrow y[k-n]$. The difference equation that is used in this model and obtained from the transfer function in (31) is:

$$\begin{aligned} y[k] = \Bigg(&-\sum_{m=1}^{n} a_{n-m} \cdot y[k-m] \\ &+ \sum_{m=0}^{n} b_{n-m} \cdot u[k-m] \Bigg) \cdot a_n^{-1} \end{aligned} \tag{32}$$

This method is simple and creative because all the previous steps should be done only once for a given system to get the coefficients $[a_0, a_1, \dots a_n$ and $b_0, b_1, \dots b_n]$. As mentioned before, those coefficients relate the output at any sample time with the outputs at previous samples and the input at current and past samples. Since system parameters are constant, then the temperature profile of the cable can be calculated very easily and fast using (32) instead of the differential equations system represented by Eqs. (27) and (28).

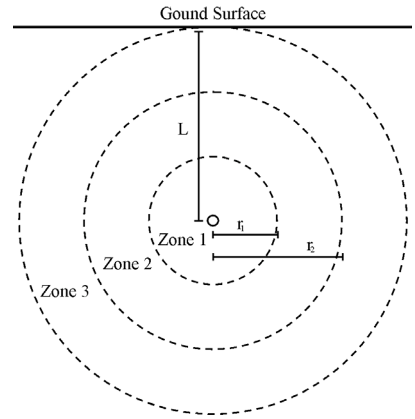

Fig. 2. The division of soil into layers of equal distance [24].

3.4. Model of cables directly buried in soil

The presented approach has the intrinsic feature of improving model accuracy at the cost of longer computation times. A more precise assessment of the temperature profile may be obtained by splitting the individual non-conducting layers (especially soil) into multiple sections [24,25,31,33,43]. The distance from the ground surface to the cable surface is divided into layers with equal distance from each other as shown in Fig. 2, where the soil is divided into 3 layers for simplicity. In reality, thermal inertia is uniformly distributed across the medium, so temperature changes gradually and reaches a steady state. To accurately model this, a minimum number of layers are necessary to distribute the thermal inertia of the soil and achieve precise dynamic results. This feature is advantageous because it allows the user to choose a suitable level of accuracy while maintaining fast computational speed. Fig. 3 shows the thermal circuit model of a DC cable buried directly in soil with multiple soil layers.

The thermal capacitance of each internal layer of the cable is calculated as shown in these equations:

$$C_c = \frac{\pi}{4} \cdot d_c^2 \cdot c_{pc} \tag{33}$$

$$C_i = \frac{\pi}{4}(d_i^2 - d_c^2) c_{pi} \tag{34}$$

$$C_s = \frac{\pi}{4}(d_s^2 - d_i^2) c_{ps} \tag{35}$$

$$C_j = \frac{\pi}{4}(D_e^2 - d_s^2) c_{pj} \tag{36}$$

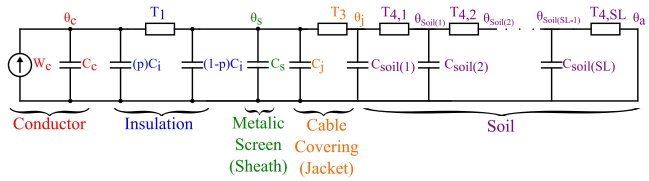

Fig. 3. Thermal circuit of a DC cable directly buried in soil with multiple soil layers.

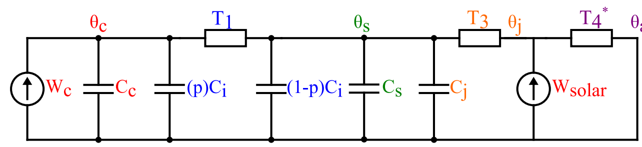

Fig. 4. Thermal circuit of a DC cable in air.

The volumetric specific heat of the conductor, insulation, sheath, and jacket are denoted by c_{pc}, c_{pi}, c_{ps}, and c_{pj}, respectively. Van Wormer suggested a technique for distributing the thermal capacity of the insulation between the conductor and the sheath to represent all the heat stored in the insulation. This technique has been found to increase the accuracy of the approximation. The Van Wormer coefficient p is calculated as:

$$p = \frac{1}{2ln\left(\frac{d_i}{d_c}\right)} - \frac{1}{\left(\frac{d_i}{d_c}\right)^2 - 1} \tag{37}$$

The thermal capacitance of the soil is represented by a cylinder with a radius equal to the laying depth and centered at the center of the cable in the model. In practice, heat will mostly move toward the surface of the ground, but in the model, heat is assumed to be distributed symmetrically away from the cable. This difference in assumptions means that the cylindrical approximation of the thermal capacitance of the soil will overestimate the actual thermal capacitance [24]. For a model with multiple soil layers, the thermal capacitance and resistance of any layer k ($1 \le k \le SL$) can be calculated using the following equations:

$$T_{4,k} = \frac{\rho_{soil}}{2\pi}\left(\ln\left(\frac{r_{ext}}{r_{int}}\right) + \frac{\ln(2)}{SL}\right) \tag{38}$$

$$C_{soil(k)} = \pi \cdot c_{psoil} \cdot (r_{ext}^2 - r_{int}^2) \tag{39}$$

Even if all soil layers have the same thickness, their thermal resistances, and capacitances will not be equal. The thermal resistance and capacitance of a soil layer k ($1 \le k \le SL$) can be calculated using the volumetric specific heat of soil, the external and internal radii of the layer, and the number of soil layers. It worth noticing that summing all the thermal resistances ($\sum_{k=1}^{SL} T_{4,k}$) will give the same result as (22).

In order to solve the circuit of Fig. 3 mathematically, the system is represented by the following set of differential equations:

$$\begin{cases} \dot{\theta}_c = \frac{1}{C_1}\left(W_c - \frac{\theta_c - \theta_s}{T_1}\right) \\ \dot{\theta}_s = \frac{1}{C_3}\left(\frac{\theta_c - \theta_s}{T_1} - \frac{\theta_s - \theta_j}{T_3}\right) \\ \dot{\theta}_j = \frac{1}{C_{soil(1)}}\left(\frac{\theta_s - \theta_j}{T_3} - \frac{\theta_j - \theta_{soil(1)}}{T_{4,1}}\right) \\ \dot{\theta}_{soil(1)} = \frac{1}{C_{soil(2)}}\left(\frac{\theta_j - \theta_{soil(1)}}{T_{4,1}} - \frac{\theta_{soil(1)} - \theta_{soil(2)}}{T_{4,2}}\right) \\ \vdots \\ \dot{\theta}_{soil(SL-1)} = \frac{1}{C_{soil(SL)}}\left(\frac{\theta_{soil(SL-2)} - \theta_{soil(SL-1)}}{T_{4,SL-1}} - \frac{\theta_{soil(SL-1)}}{T_{4,SL}}\right) \end{cases} \tag{40}$$

The parallel thermal capacitances are added together such that $C_1 = C_c + p\,C_i$ and $C_3 = C_s + (1-p)C_i + C_j$. The system of (40) can be written in state-space representation and then the difference equation of the system will be obtained. For the simplest case where there is only one soil layer (as in Fig. 1), the state-space representation of the system after substituting in (27) and (28) will be:

$$\begin{bmatrix} \dot{\theta}_c \\ \dot{\theta}_s \\ \dot{\theta}_j \end{bmatrix} = \begin{bmatrix} -\frac{1}{C_1T_1} & \frac{1}{C_1T_1} & 0 \\ \frac{1}{C_3T_1} & -\left(\frac{1}{C_3T_1} + \frac{1}{C_3T_3}\right) & \frac{1}{C_3T_3} \\ 0 & \frac{1}{C_4T_3} & -\left(\frac{1}{C_4T_4} + \frac{1}{C_4T_3}\right) \end{bmatrix} \cdot \begin{bmatrix} \theta_c \\ \theta_s \\ \theta_j \end{bmatrix} + \begin{bmatrix} \frac{1}{C_1} \\ 0 \\ 0 \end{bmatrix} \cdot \begin{bmatrix} W_c \end{bmatrix} \tag{41}$$

$$\mathbf{y} = \begin{bmatrix} 1 & 0 & 0 \end{bmatrix} \cdot \begin{bmatrix} \theta_c \\ \theta_s \\ \theta_j \end{bmatrix} + \begin{bmatrix} 0 \end{bmatrix} \cdot \begin{bmatrix} W_c \end{bmatrix} \tag{42}$$

Where $C_4 = C_{soil}$. (42) presents the case where the only wanted output is the conductor temperature.

3.5. Cables in air

There are some changes in the thermal circuit in the case of cables in the air. Since the capacitance of open air is very large, it can be ignored so $C_m = 0$. In addition, solar heat is considered a second input to the system. The thermal circuit of a DC cable in the air is shown in Fig. 4. If the cable is in shade then $W_{solar} = 0$. Unlike cables installed underground, the thermal resistance of above-ground cables (T_4^*) is presented by only one layer.

In order to solve the circuit of Fig. 4 mathematically, the system is represented by the following set of differential equations:

$$\begin{cases} \dot{\theta}_c = \frac{1}{C_1}\left(W_c - \frac{\theta_c - \theta_s}{T_1}\right) \\ \dot{\theta}_s = \frac{1}{C_3}\left(\frac{\theta_c - \theta_s}{T_1} - \frac{\theta_s}{T_3 + T_4^*} + \frac{T_4^*}{T_3 + T_4^*}W_{solar}\right) \end{cases} \tag{43}$$

The state-space representation of this system when the only wanted output is conductor temperature:

$$\begin{bmatrix} \dot{\theta}_c \\ \dot{\theta}_s \end{bmatrix} = \begin{bmatrix} -\frac{1}{C_1T_1} & \frac{1}{C_1T_1} \\ \frac{1}{C_3T_1} & -\left(\frac{1}{C_3T_1} + \frac{1}{C_3(T_3+T_4^*)}\right) \end{bmatrix} \cdot \begin{bmatrix} \theta_c \\ \theta_s \end{bmatrix} + \begin{bmatrix} \frac{1}{C_1} & 0 \\ 0 & \frac{T_4^*}{C_3(T_3+T_4^*)} \end{bmatrix} \cdot \begin{bmatrix} W_c \\ W_{solar} \end{bmatrix} \tag{44}$$

$$\mathbf{y} = \begin{bmatrix} 1 & 0 & 0 \end{bmatrix} \cdot \begin{bmatrix} \theta_c \\ \theta_s \\ \theta_j \end{bmatrix} + \begin{bmatrix} 0 & 0 \end{bmatrix} \cdot \begin{bmatrix} W_c \\ W_{solar} \end{bmatrix} \tag{45}$$

3.6. Cables in ducts or pipes

In the case of cables in ducts or pipes, two extra layers will be added to the general cable TEE of Fig. 1. Those layers are for the air between the cable and duct (or pipe), and the duct (or pipe) itself. As mentioned previously, if the duct is metal, its thermal resistivity can be ignored ($T_4'' = 0$). Fig. 5 shows a schematic of the thermal circuit of a DC cable in a duct (or pipe) either installed underground or in the air. For the sake of simplicity, only one soil layer is presented, but similar to the directly buried cable case, the soil layer can be divided into multiple layers. The difference equation can be obtained using the same procedure as section 4.3.2. The simplest case when the duct is installed underground will have five state-space variables $\mathbf{x} = \begin{bmatrix} \theta_c & \theta_s & \theta_j & \theta_{air} & \theta_{duct} \end{bmatrix}^T$. Nevertheless, if the duct is installed above ground, the model will always have four state-space variables $\mathbf{x} = \begin{bmatrix} \theta_c & \theta_s & \theta_j & \theta_{air} \end{bmatrix}^T$.

4. Model testing and result analysis

In this section, the developed thermal model for the traction network will be tested. This model is built using MATLAB. Since there are two different models incorporated into the proposed thermal mode, two types of tests are required; bare overhead lines and cables.

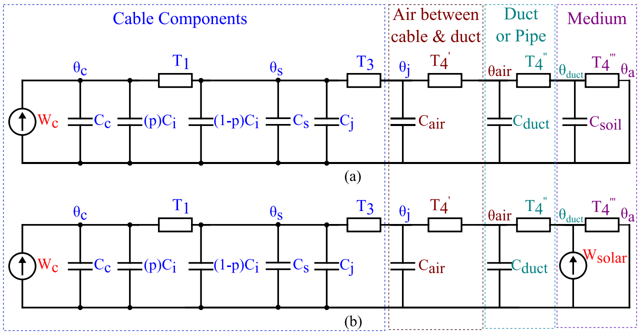

Fig. 5. Thermal circuit of a DC cable inside a duct or pipe located: (a) Underground, (b) Above ground.

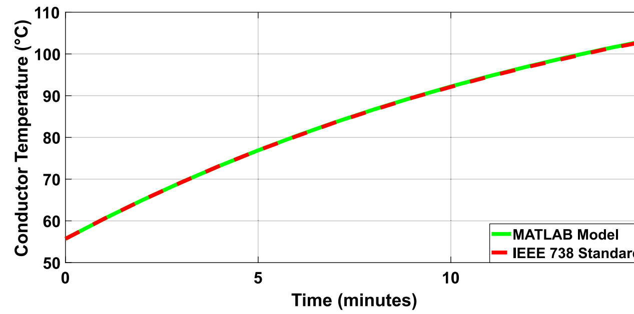

Fig. 6. Comparison of the conductor temperature between the implemented MATLAB model and IEEE 738 example.

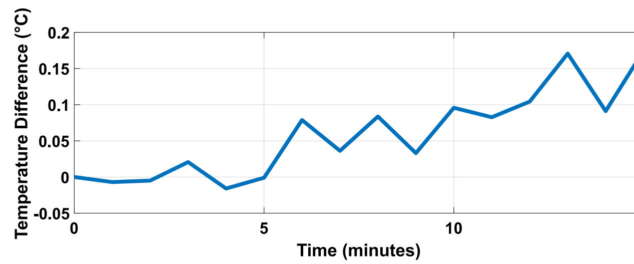

Fig. 7. Error between MATLAB model and IEEE 738 Standard for a step current input.

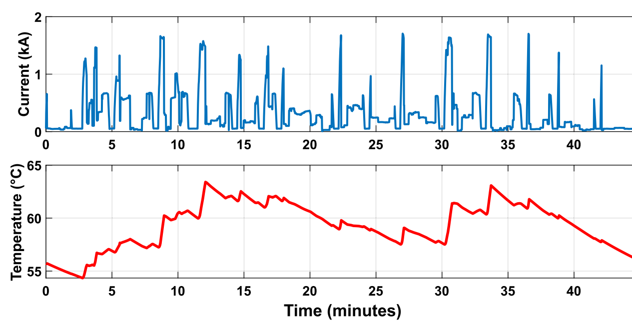

Fig. 8. Temperature profile for a varying current.

Table 2
Bare overhead model test system parameters.

Parameter	Value	Unit
Current step	1200	A
Duration of current step	15	minutes
calculation time interval	60	seconds
Ambient temperature	40	°C
Initial conductor temperature	55.7	°C
Wind speed	0.61	m/s
Angle between wind and conductor	90	degree
Conductor diameter	28.12	mm
Minimum conductor temperature	25	°C
Maximum conductor temperature	75	°C
Minimum conductor resistance	0.07284	Ω/km
Maximum conductor temperature	0.08689	Ω/km
Number of conductor materials	2	–
Heat capacity of core material	243	J/m °C
Heat capacity of outer material	1066	J/m °C
Conductor emissivity	0.5	–
Solar absorptivity	0.5	–
Elevation of conductor above sea level	0	m
Azimuth of conductor from North	45	degree
Conductor latitude	43	degree
Solar hour	12	–
Day of year	161	–
Air clarity	Clear	–

4.1. Bare overhead line model

To test the implemented MATLAB model of the bare overhead line, a numerical example of dynamic analysis of a bare overhead line is found in Annex D of IEEE 738 standard [44]. This example is chosen because the model implemented is acquired from the standard without any added contribution from the authors. The conductor type is (400 mm^2 DRAKE 26/7 ACSR), and the inputs are listed in Table 2.

A comparison of the step response of the developed MATLAB model and IEEE 738 standard results is illustrated in Fig. 6. The error between them is shown in Fig. 7. From this curve, the maximum difference is 0.175 °C (0.17% error), which is a very small difference. Thus, IEEE 738 model is accurately implemented in the proposed thermal model.

In addition, a simulation has been done in Railenos software, which is a solver for railway traction networks developed by LEMUR Research Group at the University of Oviedo. A varying current from this simulation is given as input to the model to test its outcome. Other parameters are kept similar to the previous test. The current and conductor's temperature are plotted in Fig. 8. The response seems reasonable and expected. When there are spikes in the current, the temperature tends to increase at a rate that depends on the magnitude and width of the spike.

4.2. Underground cable system

In this section, the accuracy of the proposed model using difference equation methodology is tested. In addition, the effects of adding more soil and insulation layers are investigated. All the tests are done using "Cable Number 1" from [43], and the model inputs that relate to the cable and its environment are listed in Table 3. The methods that are used to confirm the accuracy of the proposed model are; "Simulink", and "lsim tool" in MATLAB. The circuits discussed in the previous sections have been built in Simulink to test the response of the system to a given input. Moreover, from the state-space representation of those circuits, the lsim tool can produce the time response of a dynamic system to arbitrary inputs. The Simulink response is trusted to be very accurate, thus it is used as a reference to observe the errors of the other two methods.

4.2.1. Step response

A current step of 950 A is given as an input to the model of Fig. 3 considering the simplest case of one soil layer. The results are shown in Fig. 9. It is obvious that the proposed method produces very accurate results in the case of a step response. The errors of the difference equation method and lsim tool are illustrated in Fig. 10, considering Simulink response as a reference. It is clear from the figure that the error of both methods is extremely small (less than 0.005 °C).

4.2.2. Varying current

A varying load current taken from a simulation in Railneos is used as an input to the same models. The current profile is shown previously in

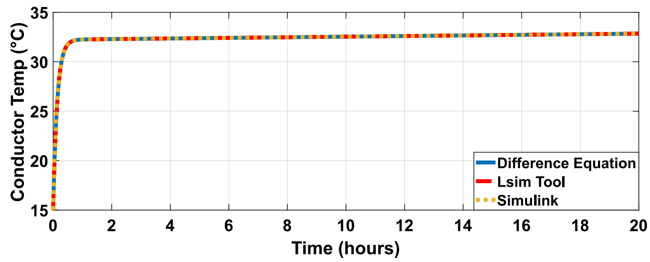

Fig. 9. Response of three models of a cable installed directly in soil to a step current of 950 A.

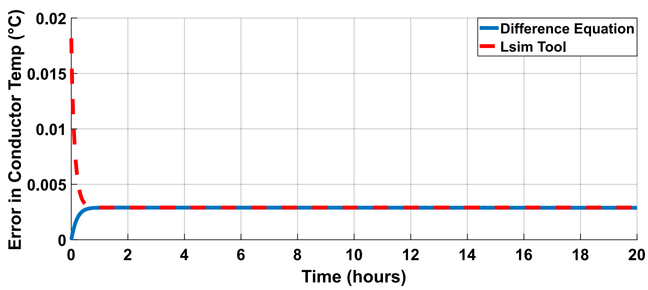

Fig. 10. Errors of the results from the response shown in (Fig. 9) compared to Simulink model.

Table 3
Cable model test system parameters.

Parameter	Value	Unit
Thermal resistivity of insulation	3.5	K m/W
Thermal resistivity of jacket	5	K m/W
Thermal resistivity of soil	1	K m/W
Volumetric specific heat of conductor	3.35	MJ/K m^3
Volumetric specific heat of insulation	2	MJ/K m^3
Volumetric specific heat of sheath	1.47	MJ/K m^3
Volumetric specific heat of jacket	1.7	MJ/K m^3
Volumetric specific heat of soil	2	MJ/K m^3
Diameter of conductor	20.5	mm
Diameter of insulation	30.1	mm
Diameter of sheath	31.4	mm
Diameter of jacket	35.8	mm
Ground distance to the cable axis	1	m
Cross-sectional area of conductor	300	mm^2
Thermal coefficient at 20 °C	0.00393	1/°C
Electric resistivity of conductor	$1.724/10^8$	Ω m
Maximum conductor temperature	90	°C
Intensity of solar radiation	1000	W/m^2
Absorption coefficient of cable surface	0.6	–
Ambient temperature	15	°C
Initial conductor temperature	15	°C
Time step	1	second rule

Fig. 8. The results are shown in Fig. 11. It is obvious that the proposed method produces very accurate results in the case of variable loading as well. The errors of the difference equation method and lsim tool are illustrated in Fig. 12, considering Simulink response as a reference. It is clear from the figure that the difference equation method performance is even better than the lsim tool, however, the latter method still provides a very good response with a maximum error of less than 0.06 °C.

4.2.3. Effects of multiple soil layers

Since the accuracy of the proposed method and lsim tool is proven, for the sake of this part, the proposed method will not be used. Instead, lsim and Simulink will be used as they are easier and faster to simulate multiple models. The simulations are done for a current step of 950 A in three models; single layer, 5 layers, and 50 layers. The outcomes

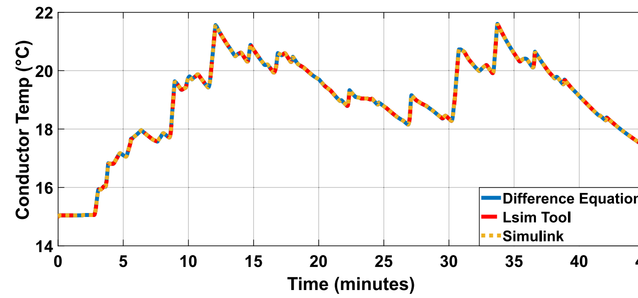

Fig. 11. Response of a cable installed directly in soil to a variable current profile.

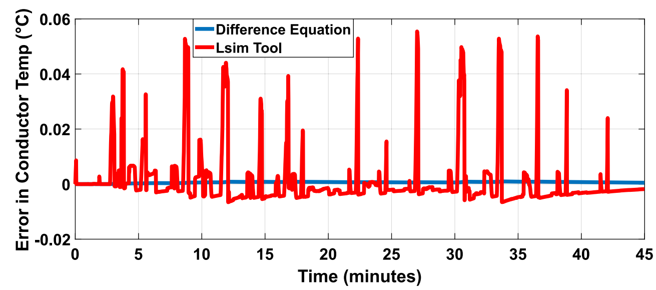

Fig. 12. Errors of the results from the response shown in (Fig. 11) compared to Simulink model.

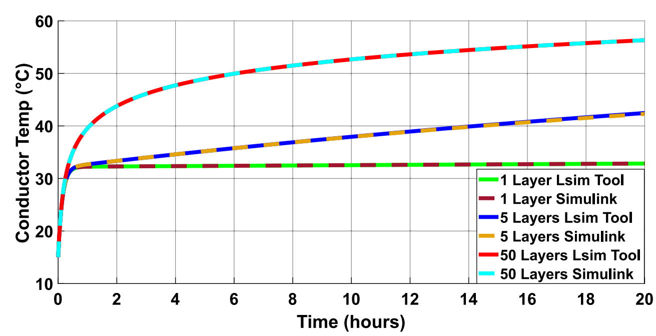

Fig. 13. Effect of multiple numbers of soil layers on dynamic time response to a step current of 950 A.

are presented in Fig. 13. It can be concluded that dividing the soil into multiple layers has major effects on the shape and magnitude of the resulting time response, and the more layers the more accurate the simulation will be. It is proven again that the lsim tool is reliable in simulating dynamic systems. Since the scope of this paper is only concerned with railways, then it is more important to test the effects of multiple soil layers on Railneos variable current signal. For better visualization, the lsim tool only is used to simulate the model at 1, 10, 50, 100, and 200 layers. The results are shown in Fig. 14. It can be noticed that the differences are not as huge as it was in the case of the current step. However, both tests show that the temperature profile is higher in magnitude when more layers are used. This concludes that using only one layer of soil underestimates the true thermal behavior. The errors produced when using less than 200 layers compared to the 200 layers response are plotted in Fig. 15. This figure demonstrates the flexibility of the TEE method. Depending on the application intended, the TEE approach can give accuracy that satisfies the requirements and within simulation time lesser than FEM and other TEE applications with more layers.

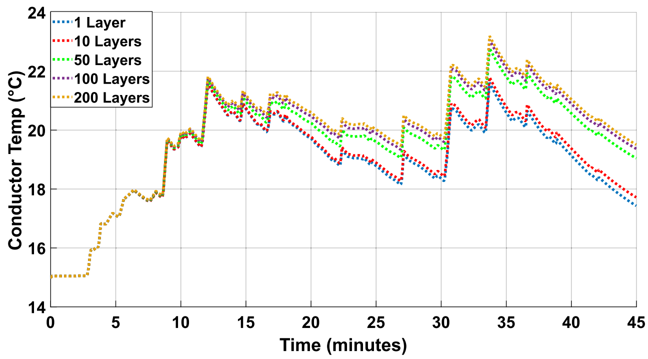

Fig. 14. Effect of multiple numbers of soil layers on dynamic time response to a variable current.

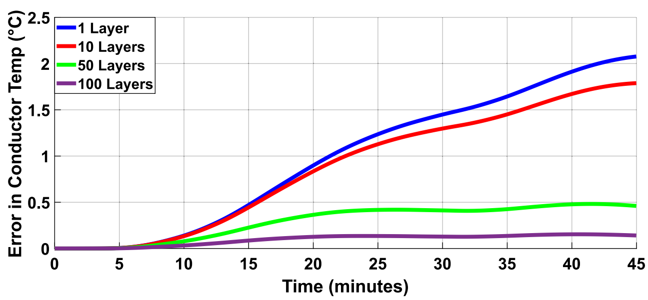

Fig. 15. Temperature errors produced when simulating less than 200 layers compared to 200 layers' results.

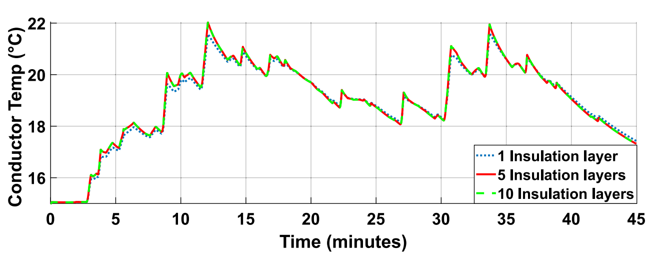

Fig. 16. Effect of multiple numbers of insulation layers on dynamic time response to a variable current.

4.2.4. Effects of multiple insulation layers

Some researchers in the literature have divided the insulation layer into multiple layers to increase the accuracy, such as the model presented in [25]. Using the lsim tool, a simulation has been done with 1, 5, and 10 layers under variable loading as seen in Fig. 16. The difference between a single layer and 5 layers is small (the maximum difference is around 0.2 °C). Adding more than 5 layers will result in the same response, for example, a simulation with 200 layers has been done and the results are approximately equal to the result of 5 layers. This concludes that adding more insulation layers increases simulation time without major effects on the response.

4.3. Above-ground cable system

In cable systems installed in the air either exposed or inside a duct, solar radiation plays an important role in shaping the temperature gradient. In addition, the way temperature dissipated to air is different from the case of ground. Thus, it is expected that the response of the same cable will differ. In this section, the circuit of Fig. 4 is simulated to see those effects and to confirm the accuracy of the proposed model.

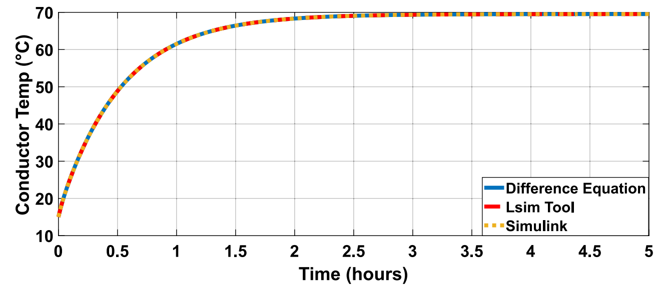

Fig. 17. Response of three models of a cable in air not exposed to the sun to a step current of 950 A.

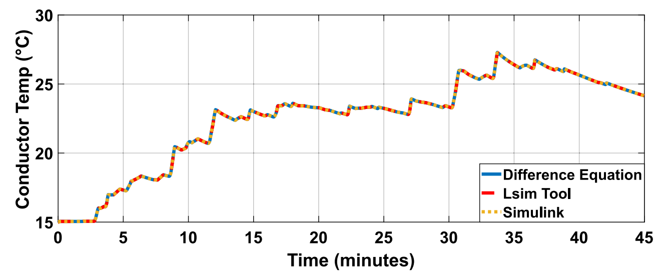

Fig. 18. Response to a variable current of three models of a cable in air not exposed to the sun.

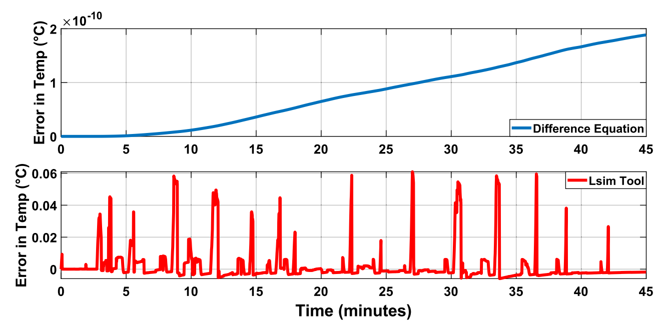

Fig. 19. Errors of the results from the response shown in (Fig. 18) compared to Simulink model.

4.3.1. Cables not exposed to the sun

The test simulations have been run when $W_{solar} = 0$ by using the proposed method, slim tool, and Simulink circuit. The time response to a step current of 950 A is plotted in Fig. 17, while the time response to a variable Railneos current is shown in Fig. 18. Comparing Fig. 17 with Fig. 9, and Fig. 18 with Fig. 11, it is obvious that there are differences in the shape of response and magnitude of temperature. This is mainly because the dominant heat dissipation method is conduction for underground installations, whereas, it is convection and radiation in above-ground installations. From Figs. 17 and 18, the accuracy of the proposed difference equation method and lsim tool is confirmed. The error of both methods in the case of varying current is illustrated in Fig. 19, considering Simulink response as a reference. From this figure, It is clear that the difference equation method performance is far better than the lsim tool, however, the latter method still provides a very good response with a maximum error of less than 0.06 °C.

4.3.2. Cables exposed to the sun

The system is simulated when $W_{solar} \neq 0$ under varying current extended to 3 h to get the maximum error. Fig. 20 shows the response of the difference equation method, lsim tool, and Simulink model to this varying current. The response is quite similar, however, Simulink's response is a little bit greater in magnitude. Fig. 21 illustrates the

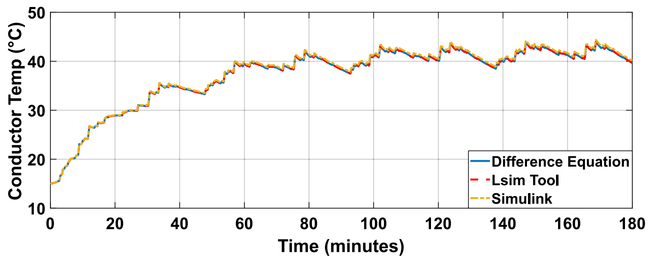

Fig. 20. Response to a variable current of three models of a cable in air exposed to the sun.

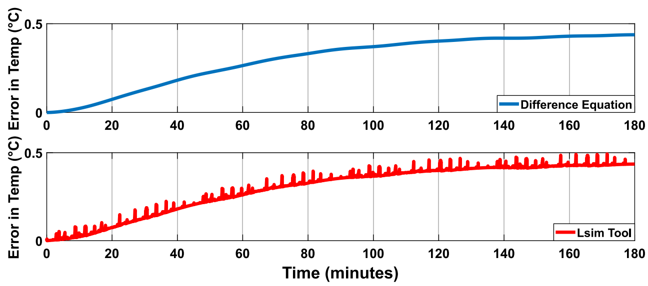

Fig. 21. Errors of the results from the response shown in (Fig. 20) compared to Simulink model.

differences in magnitude between Simulink response and the other methods. The error, in this case, is greater than in all the previous cases. However, the maximum error reached is 0.5 °C, which is not very significant for most of the applications. It is worth mentioning that the difference equation method response is more stable than lsim as seen from the fluctuation in Fig. 12, Fig. 19 and Fig. 21.

5. Conclusion

Dynamic thermal analysis helps to utilize electrical conductors to their actual potential and avoids conductor overloading, thus increasing the reliability of electric networks. This work is focused on the conductors of a DC traction network. Out of many procedures and methods of calculating the temperature profile of conductors, the most accurate and efficient methods have been chosen to be implemented in this paper. For bare overhead lines, IEEE 738 standard technique is modeled. The numerical thermal model presented in this standard is very general. It is applicable for steady-state or dynamic calculations. In this method, all important factors are considered without simplifications. The model is tested using a case study in the same standard. For insulated cables, another method is used called thermo-electric equivalents (TEEs), also denoted as lumped parameters model. Its accuracy can be as good as FEM, and its simulation speed is as fast as analytical calculations. The "Difference Equation" methodology is utilized to transfer complicated differential equations into simpler linear equations. The model has been verified using a thermal circuit modeled in Simulink and a MATLAB tool called "lsim", and the results were accurate.

6. Future directions

The models developed in this paper are all verified using other simulation tools. Thus, the accuracy of these models should be tested further by using experimental measurements or at least compared to FEM-based software, such as ANSYS or COSOL Multiphysics. In addition, the simulation speed and accuracy of the models could be enhanced by using new methods or developing the proposed ones. Distributing computing could be a very promising technique to use in the development of thermal models, and it might increase the scope, simulation speed, and accuracy.

CRediT authorship contribution statement

Mohammed G. Mahairi: Writing – review & editing, Writing – original draft, Methodology, Formal analysis, Data curation. **Bassam Mohamed:** Writing – review & editing, Writing – original draft, Supervision, Methodology, Investigation, Conceptualization. **Pablo Arboleya:** Writing – review & editing, Writing – original draft, Supervision, Project administration, Conceptualization.

Declaration of competing interest

The authors declare that they have no known competing financial interests or personal relationships that could have appeared to influence the work reported in this paper.

Data availability

The data that has been used is confidential.

References

[1] UIC and CER, Rail Transport and Environment: Facts and Figures, UIC-ETF (Railway Techincal Publications), 2015.
[2] P. Chatzipanagiotou, V. Chatziathanasiou, Dynamic thermal analysis of a power line by simplified RC model networks: Theoretical and experimental analysis, Int. J. Electr. Power Energy Syst. 106 (2019) 288–293, [Online]. Available: https://www.sciencedirect.com/science/article/pii/S0142061518316119.
[3] G. Liu, B. Ruan, M. Zhang, A transient model for overhead transmission line dynamic rating based on thermal circuit method, Autom. Electr. Power Syst. 36 (16) (2012) 58–62.
[4] G. Liu, B. Ruan, J. Lin, M. Yang, M. Zhang, Z. Xu, Steady-state model of thermal circuit method for dynamic overhead lines rating, High Voltage Eng. 39 (5) (2013) 1107–1113.
[5] X. Zhang, Z. Ying, Y. Chen, X. Chen, A thermal model for calculating axial temperature distribution of overhead conductor under laboratory conditions, Electr. Power Syst. Res. 166 (2019) 223–231, [Online]. Available: https://www.sciencedirect.com/science/article/pii/S0378779618303250.
[6] Y. Zhanfeng, F.K. Du Zhijia, et al., Radial thermal circuit model and parameter calculation method for high voltage overhead transmission line, Trans. China Electrotech. Soc. 31 (4) (2016) 13–21.
[7] Y. Zhanfeng, F. Kai, D. Zhijia, Thermal circuit modeling of the relationship between current and axial temperature for high voltage overhead conductor, Proc. CSEE 35 (11) (2015) 2887–2895.
[8] I. Makhkamova, K. Mahkamov, P. Taylor, CFD thermal modelling of lynx overhead conductors in distribution networks with integrated renewable energy driven generators, Appl. Therm. Eng. 58 (1) (2013) 522–535, [Online]. Available: https://www.sciencedirect.com/science/article/pii/S1359431113003372.
[9] S. Maximov, V. Venegas, J. Guardado, E. Moreno, R. López, Analysis of underground cable ampacity considering non-uniform soil temperature distributions, Electr. Power Syst. Res. 132 (2016) 22–29, [Online]. Available: https://www.sciencedirect.com/science/article/pii/S0378779615003314.
[10] J. Nahman, M. Tanaskovic, Calculation of the loading capacity of high voltage cables laid in close proximity to heat pipelines using iterative finite-element method, Int. J. Electr. Power Energy Syst. 103 (2018) 310–316, [Online]. Available: https://www.sciencedirect.com/science/article/pii/S0142061517333355.
[11] C. Garrido, A. Otero, J. Cidras, Theoretical model to calculate steady-state and transient ampacity and temperature in buried cables, IEEE Trans. Power Deliv. 18 (3) (2003) 667–678.
[12] M. Hanna, A. Chikhani, M. Salama, Thermal analysis of power cable systems in a trench in multi-layered soil, IEEE Trans. Power Deliv. 13 (2) (1998) 304–309.
[13] J. Nahman, M. Tanaskovic, Determination of the current carrying capacity of cables using the finite element method, Electr. Power Syst. Res. 61 (2) (2002) 109–117, [Online]. Available: https://www.sciencedirect.com/science/article/pii/S0378779602000032.
[14] L. Jenkins, N. Fahmi, J. Yang, Application of dynamic asset rating on the UK LV and 11 kV underground power distribution network, in: 2017 52nd International Universities Power Engineering Conference, UPEC, 2017, pp. 1–6, http://dx.doi.org/10.1109/UPEC.2017.8231879.
[15] M. Al-Saud, Assessment of thermal performance of underground current carrying conductors, IET Gener., Transm. Distribution 5 (2011) 630–639(9), [Online]. Available: https://digital-library.theiet.org/content/journals/10.1049/iet-gtd.2010.0258.
[16] D. Lauria, M. Pagano, C. Petrarca, Transient thermal modelling of HV XLPE power cables: matrix approach and experimental validation, in: 2018 IEEE Power Energy Society General Meeting, PESGM, 2018, pp. 1–6, http://dx.doi.org/10.1109/PESGM.2018.8586514.

[17] S.L. Roy, T. Vu, G. Teyssedre, Modelling charge transport in a HVDC cable using different softwares: from fluid models to macroscopic model, in: 2019 2nd International Conference on Electrical Materials and Power Equipment, ICEMPE, 2019, pp. 337–340, http://dx.doi.org/10.1109/ICEMPE.2019.8727386.

[18] J.A. Souza, J.C. Ordonez, R. Hovsapian, J.V.C. Vargas, Thermal modeling of helium cooled high-temperature superconducting DC transmission cable, IEEE Trans. Appl. Supercond. 21 (3) (2011) 947–952.

[19] N.G. Suttell, J.V. Coelho Vargas, J.C. Ordonez, Transient thermal analysis of HTS DC cables cooled with gaseous helium using a volume element method, IEEE Trans. Appl. Supercond. 27 (4) (2017) 1–5.

[20] X. Ding, L. Ren, X. Li, Y. Xu, T. Feng, Z. Yang, J. Shi, M. Song, L. Li, J. Li, Y. Tang, Thermal characteristics of gaseous-helium-cooled HTS cables with practical operating conditions, IEEE Trans. Appl. Supercond. 32 (8) (2022) 1–7.

[21] J.C. Ordonez, J.A. Souza, D.R. Shah, J.V.C. Vargas, R. Hovsapian, Temperature and pressure drop model for gaseous helium cooled superconducting DC cables, IEEE Trans. Appl. Supercond. 23 (3) (2013) 5402005.

[22] G. Chen, L. Ren, H. Huang, Y. Xu, X. Li, J. Li, J. Shi, Y. Tang, Thermal analysis of tri-axial HTS cable, in: 2021 IEEE 4th International Electrical and Energy Conference, CIEEC, 2021, pp. 1–5, http://dx.doi.org/10.1109/CIEEC50170.2021.9510660.

[23] D.I. Doukas, T.A. Papadopoulos, A.I. Chrysochos, D.P. Labridis, G.K. Papagiannis, Multiphysics modeling for transient analysis of gas-insulated lines, IEEE Trans. Power Deliv. 33 (6) (2018) 2786–2793.

[24] R.S. Olsen, J. Holboll, U.S. Gudmundsdóttir, Dynamic temperature estimation and real time emergency rating of transmission cables, in: 2012 IEEE Power and Energy Society General Meeting, 2012, pp. 1–8, http://dx.doi.org/10.1109/PESGM.2012.6345324.

[25] R. Olsen, G.J. Anders, J. Holboell, U.S. Gudmundsdóttir, Modelling of dynamic transmission cable temperature considering soil-specific heat, thermal resistivity, and precipitation, IEEE Trans. Power Deliv. 28 (3) (2013) 1909–1917.

[26] B. Mohamed, P. Arboleya, C. González-Morán, Modified current injection method for power flow analysis in heavy-meshed DC railway networks with nonreversible substations, IEEE Trans. Veh. Technol. 66 (9) (2017) 7688–7696.

[27] P. Arboleya, B. Mohamed, I. El-Sayed, DC railway simulation including controllable power electronic and energy storage devices, IEEE Trans. Power Syst. 33 (5) (2018) 5319–5329.

[28] IEEE, IEEE standard for calculating the current-temperature relationship of bare overhead conductors, IEEE Std 738-2023 (Revision of IEEE Std 738-2012), 2023, pp. 1–56.

[29] H.E. House, P.D. Tuttle, Current-carrying capacity of ACSR, Trans. Am. Inst. Electr. Eng. III 77 (3) (1958) 1169–1173.

[30] Y.A. Cengel, M.A. Boles, Thermodynamics: An Engineering Approach, McGraw-Hill Education, 2014.

[31] G.J. Anders, Rating of Electric Power Cables in Unfavorable Thermal Environment, Wiley-IEEE Press, 2005.

[32] D. Enescu, P. Colella, A. Russo, Thermal assessment of power cables and impacts on cable current rating: An overview, Energies 13 (20) (2020) [Online]. Available: https://www.mdpi.com/1996-1073/13/20/5319.

[33] M. Diaz-Aguiló, F. De León, S. Jazebi, M. Terracciano, Ladder-type soil model for dynamic thermal rating of underground power cables, IEEE Power Energy Technol. Sys. J. 1 (2014) 21–30.

[34] R. Zhang, H. Sun, X. Dong, The comparison of thermal characteristics of AC cable and DC cable, J. Phys. Conf. Ser. 1187 (2) (2019) 022051.

[35] P. Wang, L. Kang, Z. Xu, W. Zhou, S. Bao, Z. Wu, Y. Hao, G. Liu, Dynamic thermal analysis for underground cables under continuously fluctuant load considering time-varying van wormer coefficient, Electr. Power Syst. Res. 199 (2021) 107395, [Online]. Available: https://www.sciencedirect.com/science/article/pii/S037877962100376X.

[36] O.E. Gouda, G.F.A. Osman, Enhancement of the thermal analysis of power cables installed in polyvinyl chloride (PVC) ducts under continuous and cyclic current loading conditions, IET Gener., Transm. Distribution 15 (7) (2021) 1144–1158, [Online]. Available: https://ietresearch.onlinelibrary.wiley.com/doi/abs/10.1049/gtd2.12092.

[37] R.S. Singh, S. Cobben, V. Ćuk, PMU-based cable temperature monitoring and thermal assessment for dynamic line rating, IEEE Trans. Power Deliv. 36 (3) (2021) 1859–1868.

[38] M. Hruška, C. Clauser, R.W. De Doncker, Influence of dry ambient conditions on performance of underground medium-voltage DC cables, Appl. Therm. Eng. 149 (2019) 1419–1426, [Online]. Available: https://www.sciencedirect.com/science/article/pii/S1359431118339784.

[39] A. Shekhar, X. Feng, R. Hebner, A. Gattozzi, S. Strank, A. Mor, L. Ramirez-Elizondo, P. Bauer, Thermal modelling and experimental validation for research on medium voltage DC cables, in: 2017 IEEE Power and Energy Society General Meeting, PESGM 2017, 2018-January, 2018, pp. 1–5, http://dx.doi.org/10.1109/PESGM.2017.8274559.

[40] S. Gasnier, A. André, S. Poullain, V. Debusschere, B. Francois, P. Egrot, Models of AC and DC cable systems for technical and economic evaluation of offshore wind farm connection, Int. J. Electr. Energy 6 (2) (2018) 64–73.

[41] IEC, Electric cables—Calculation of the current rating—Part 2: Thermal resistance—Section 1: Calculation of the thermal resistance, IEC Standard 60287-2-1, 2015.

[42] R.L. Williams, D.A. Lawrence, Linear State-Space Control Systems, John Wiley & Sons, 2007.

[43] G.J. Anders, Rating of Electric Power Cables: Ampacity Computations for Transmission, Distribution, and Industrial Applications, Institute of Electrical & Electronics Engineers(IEEE), 1997.

[44] IEEE draft standard for calculating the current-temperature relationship of bare overhead conductors, IEEE Std 738-2012 Draft 10 (Revision of IEEE Std 738-2006), 2012, pp. 1–67.